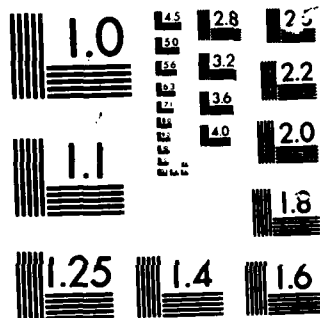


MOLECULAR REACTION RATES(U) WISCONSIN UNIV-MADISON DEPT 1/1
OF PHYSICS C C LIN ET AL. 28 OCT 85 AFGL-TR-85-0262
F19628-82-C-0042

F/G 7/4

144

[illegible]



MICROCOPY

CHART

AFGL-TR-85-0262

MOLECULAR REACTION RATES

Chun C. Lin
Sunggi Chung

Department of Physics
University of Wisconsin-Madison
Madison, Wisconsin 53706

Final Report
6 April 1982 - 30 September 1985

28 October 1985

DTIC
ELECTE
APR 15 1986
S D

Approved for public release; distribution unlimited

DTIC FILE COPY


AIR FORCE GEOPHYSICS LABORATORY
AIR FORCE SYSTEMS COMMAND
UNITED STATES AIR FORCE
HANSCOM AFB, MASSACHUSETTS 01731

This technical report has been reviewed and is approved for publication


EDWARD T.P. LEE
Contract Manager


W.A.M. BLUMBERG, Acting Chief
Infrared Dynamics Branch

FOR THE COMMANDER


RANDALL E. MURPHY, Director
Infrared Technology Division

This report has been reviewed by the ESD Public Affairs Office (PA) and is releasable to the National Technical Information Service (NTIS).

Qualified requestors may obtain additional copies from the Defense Technical Information Center. All others should apply to the National Technical Information Service.

If your address has changed, or if you wish to be removed from the mailing list, or if the addressee is no longer employed by your organization, please notify AFGL/DAA, Hanscom AFB, MA 01731. This will assist us in maintaining a current mailing list.

Do not return copies of this report unless contractual obligations or notices on a specific document requires that it be returned.

Unclassified

SECURITY CLASSIFICATION OF THIS PAGE (When Data Entered)

REPORT DOCUMENTATION PAGE		READ INSTRUCTIONS BEFORE COMPLETING FORM
1. REPORT NUMBER AFGL-TR-85-0262	2. GOVT ACCESSION NO. ADA 166518	3. RECIPIENT'S CATALOG NUMBER
4. TITLE (and Subtitle) Molecular Reaction Rates		5. TYPE OF REPORT & PERIOD COVERED Final 6 April 1982 - 30 Sept. 1985
		6. PERFORMING ORG. REPORT NUMBER
7. AUTHOR(s) Chun C. Lin Sunggi Chung		8. CONTRACT OR GRANT NUMBER(s) F 19628-82-C-0042
9. PERFORMING ORGANIZATION NAME AND ADDRESS Department of Physics University of Wisconsin-Madison Madison, Wisconsin 53706		10. PROGRAM ELEMENT, PROJECT, TASK AREA & WORK UNIT NUMBERS 61102F 2310G4AZ
11. CONTROLLING OFFICE NAME AND ADDRESS Air Force Geophysics Laboratory Hanscom AFB, Massachusetts 01731 Monitor/Edward T.P. Lee/LSI		12. REPORT DATE 28 October 1985
		13. NUMBER OF PAGES 60
14. MONITORING AGENCY NAME & ADDRESS (if different from Controlling Office)		15. SECURITY CLASS. (of this report) Unclassified
		15a. DECLASSIFICATION/DOWNGRADING SCHEDULE
16. DISTRIBUTION STATEMENT (of this Report) Approved for public release; distribution unlimited		
17. DISTRIBUTION STATEMENT (of the abstract entered in Block 20, if different from Report)		
18. SUPPLEMENTARY NOTES		
19. KEY WORDS (Continue on reverse side if necessary and identify by block number) Rydberg states, quantum defect, dissociative excitation by electron impact, optical excitation cross sections, atomic transition probabilities, ground state, ionization, Cation, electron orbitals, Hamiltonian equations, Eigen values, energy levels		
20. ABSTRACT (Continue on reverse side if necessary and identify by block number) The energies and wave functions for several series of Rydberg states of the nitrogen molecule have been calculated. Based on these results a long-wave infrared emission spectrum of the nitrogen molecule is predicted. The optical cross sections for exciting a series of atomic oxygen emission lines in the long-wave infrared region by electron impact on oxygen molecules have been obtained. Keywords: -		

Unclassified

SECURITY CLASSIFICATION OF THIS PAGE (When Data Entered)

PART I

RYDBERG STATES OF THE NITROGEN MOLECULE

1. INTRODUCTION

The Rydberg states of the N_2 molecule have long been of interest.¹ As a result of the axial symmetry of the molecule, in contrast to the spherical symmetry of atoms, one expects a wide variety of Rydberg series for N_2 . Because of the complexity of the N_2 spectrum, some predicted Rydberg series have not been observed, and there are many observed lines as yet unidentified.

In this paper we shall present theoretical calculations of the $1,3\Sigma_g^+$, $1,3\Sigma_u^+$, $1,3\Pi_g$, and $1,3\Pi_u$ Rydberg states, all converging to the ground $X^2\Sigma_g^+$ state of the N_2^+ ion. Numerous theoretical treatments of N_2 Rydberg states have appeared in the literature.²⁻⁵ All these works attempted to construct an effective one-electron Hamiltonian to solve for the Rydberg orbitals as is done in this work. In this regard Duncan and Damiani² approximated the core orbitals by one-center functions (centered at the midpoint of the two nuclei) to facilitate the calculation. Betts and McKoy³ used a model potential⁵ in the Hamiltonian. They³ used as basis functions a set of Gaussian-type orbitals (GTO) centered at various points along the nuclear axis. Lefebvre-Brion and Moser⁴ constructed the Hamiltonian by using the occupied orbitals. Their basis functions for the Rydberg states are the Slater-type orbitals centered at the two nuclear sites.

In many ways our approach parallels that of Ref. 4. However, we take the view that a Rydberg state must reflect a physical situation in which an electron moves in a nearly central field. Thus, we begin by treating a quasi-spherical molecular system (centered at the midpoint of the molecule) in which a Rydberg electron is characterized by atomic-like orbitals with angular momentum (l, m). Since this idealization is not fulfilled for the real molecular Rydberg states, we make allowance for l -mixing to obtain

the final results. Formal theory on the Rydberg states is extensively discussed by Mulliken.⁶ A detailed analysis of the molecular spectra^{6,7} requires consideration of such interactions as the coupling between the electronic motion with molecular rotation. However, we restrict our scope to the electronic part of the problem, and calculate the wave functions at the equilibrium separation $R = 1.1 \text{ \AA}$ of the $X^2 \Sigma_g^+$ state of N_2^+ .

Accession For	
NTIS CRA&I	<input checked="" type="checkbox"/>
DTIC TAB	<input type="checkbox"/>
Unannounced	<input type="checkbox"/>
Justification	
By	
Distribution /	
Availability Codes	
Dist	Avail and/or Special
A-1	



II. METHOD OF COMPUTATION

The Rydberg states converging to the ground $X^2\Sigma_g^+$ state of N_2^+ ion have the electronic configuration,

$$(1\sigma_g)^2(2\sigma_g)^2(1\sigma_u)^2(2\sigma_u)^2(1\pi_u)^4(3\sigma_g)(\psi_{Ry}). \quad (1)$$

Since the core (N_2^+) is in a $^2\Sigma_g^+$ state, Rydberg orbitals ψ_{Ry} of the type $k\sigma_g$, $k\sigma_u$, $k\pi_g$, and $k\pi_u$ give rise to the $1,3\Sigma_g^+$, $1,3\Sigma_u^+$, $1,3\Pi_g$, and $1,3\Pi_u$ states respectively. The corresponding wave functions are constructed as antisymmetrized products of these one-electron molecular orbitals (MO) e.g.,

$$\begin{aligned} \Psi(^1\Sigma_g^+) = \frac{1}{\sqrt{2}} [& |1\sigma_g(\vec{r}_1)\alpha \ 1\sigma_g(\vec{r}_2)\beta \dots 3\sigma_g(\vec{r}_{N-1})\alpha \ \psi_{\sigma_g}(\vec{r}_N)\beta| \\ & + |1\sigma_g(\vec{r}_1)\alpha \ 1\sigma_g(\vec{r}_2)\beta \dots 3\sigma_g(\vec{r}_{N-1})\beta \ \psi_{\sigma_g}(\vec{r}_N)\alpha|], \end{aligned} \quad (2)$$

where $|\dots|$ represents a determinant, and α, β are the two spin functions.

The Hamiltonian of the system is (in atomic units)

$$H = \sum_{i=1}^{14} \left[-\frac{1}{2} \nabla_i^2 - Z(|\vec{r}_i - \vec{r}_A|^{-1} + |\vec{r}_i - \vec{r}_B|^{-1}) \right] + \sum_{i>j}^{14} |\vec{r}_i - \vec{r}_j|^{-1}, \quad (3)$$

where \vec{r}_A, \vec{r}_B are the two nuclear sites and $Z(=7)$ is the nuclear charge. We adopt the frozen-core approximation, namely, we assume that the N_2^+ core orbitals are not affected by the addition of the Rydberg electron. Hence the $1\sigma_g, 2\sigma_g, 1\sigma_u, 2\sigma_u, 1\pi_u$, and $3\sigma_g$ core orbitals in Eq. (2) are obtained by the self-consistent-field (SCF) procedure⁸ for the $X^2\Sigma_g^+$ state of N_2^+ . In this SCF calculation the GTO are used as the basis functions,⁹ and the core orbitals are expanded by GTO centered at the two nuclear sites. As for the Rydberg orbitals we express them in terms of basis functions which are centered at the midpoint of N_2 , viz.,

$$\psi_{Ry} = \sum_{k\ell} c_{k\ell} u_{k\ell m}(\vec{r}), \quad (4)$$

with

$$u_{k\ell m}(\vec{r}) = \frac{1}{r} F_{k\ell m}(r) Y_{\ell m}(\hat{r}). \quad (5)$$

The notation is standard except that n is replaced by k . Our use of one-center basis functions for the outer electron differs from the works of Refs. 3 and 4 in which the basis functions consisted of molecular orbitals constructed from prechosen atomic orbitals judged to be suitable by the respective authors.

A. Basis Functions

Following the standard notation of the Hartree-Fock theory, we designate the electron-nucleus and electron-electron interaction by V and the electron exchange operator by W . For a diatomic molecule if we use the spherical harmonics as the angular part of the basis functions, as in Eq. (5), the axial nature of the diatomic molecule makes V and W diagonal in m but not in ℓ . This is reflected in the ℓ -summation that appears in the expansion of the wave functions according to Eq. (4). To ensure fast convergence of the k -summation in that expansion, we choose as the $F_{k\ell m}(r)$ functions the solution of a quasi-spherical molecular Rydberg system. In other words the $F_{k\ell m}$'s are obtained by solving the integro-differential equation

$$\left[\frac{d^2}{dr^2} - \frac{\ell(\ell+1)}{r^2} - V_{\ell m, \ell m}(r) - W_{\ell m, \ell m}(r) + \lambda_{k\ell m} \right] F_{k\ell m}(r) = 0, \quad (6)$$

where

$$\begin{aligned}
V_{\ell m, \ell' m'}(r) = & -2Z/d\hat{r} Y_{\ell m}^*(\hat{r}) Y_{\ell' m'}(\hat{r}) (|\vec{r}-\vec{r}_A|^{-1} + |\vec{r}-\vec{r}_B|^{-1}) \\
& + 2 \int d\hat{r} Y_{\ell m}^*(\hat{r}) Y_{\ell' m'}(\hat{r}) \sum_j f_j \int \phi_j^*(\vec{r}') |\vec{r}-\vec{r}'|^{-1} \phi_j(\vec{r}') d\vec{r}'. \quad (7)
\end{aligned}$$

The summation over j covers all the core orbitals ϕ_j with the respective occupation numbers f_j . The exchange potential is an integral operator, viz.,

$$\begin{aligned}
W_{\ell m, \ell' m'}(r) F_{k' \ell' m'}(r) = & -\sum_j f_j' \sum_{tg} \left[\frac{4\pi}{2t+1} \right] r \int d\hat{r} Y_{tg}^*(\hat{r}) Y_{\ell m}^*(\hat{r}) \phi_j(\vec{r}) \\
& \times \left[\{ r^{-t-1} \int_0^r r'^t F_{k' \ell' m'}(r') dr' + r^t \int_r^\infty r'^{-t-1} F_{k' \ell' m'}(r') dr' \} \right. \\
& \left. \times r' \int d\hat{r}' Y_{tg}(\hat{r}') Y_{\ell' m'}(\hat{r}') \phi_j^*(\vec{r}') \right], \quad (8)
\end{aligned}$$

where, again the summation is over the core orbitals ϕ_j with appropriate numerical coefficients f_j' . The detailed numerical procedures of computing Eqs. (7) and (8) are shown elsewhere.¹⁰ Here, we merely note that Eq. (7) is computed with no approximation, but the summation over t in Eq. (8) is an infinite series, which is truncated after five terms.

Except for the exchange term, we follow very closely the procedure of Herman and Skillman¹¹ to compute numerically $F_{k\ell m}(r)$. As to the exchange term we do not use the Slater approximation, but adopt a scheme which has been applied successfully to electron-scattering problems.^{9,12} That is, as we solve Eq. (6) iteratively for $\dots F^{(n)}$, $F^{(n+1)}$, etc. for the n -th and $(n+1)$ st sets of solutions, we approximate the integral operator as

$$W_F^{(n+1)} \approx \{ [WF^{(n)}] / F^{(n)} \} F^{(n+1)}, \quad (9)$$

except for the initial cycle where we set $WF^{(1)} = 0$. The function $WF^{(n)}$ is first computed by using the solution of the previous cycle $F^{(n)}$ as shown in Eq. (8), then divided by $F^{(n)}$. Thus, Eq. (6) remains a

homogeneous equation as in the calculation without exchange or with exchange treated by Slater's approximation. In the limit of convergence $F^{(n+1)} = F^{(n)}$ in the self-consistent iteration, Eq. (9) is justified. We have not encountered any serious numerical problems associated with dividing $WF^{(n)}$ by $F^{(n)}$. The mesh-sizes used are shown in Table I.

In this manner, we computed the radial basis functions $F_{k\ell m}$ for $k = 1-11$, $\ell = 0-9$, and $m = 0, 1$. The exchange coefficients f_j^1 appropriate for the singlet states are used. No separate set of basis functions is calculated for the triplet states.

In Tables II-V we list the values of $\lambda_{k\ell m}$ which are the eigenvalues of the quasi-spherical Rydberg molecule. For large values of k , we expect $\lambda_{k\ell m}$ to approximate fairly well the Rydberg levels. In this paper, of course, we do not take $F_{k\ell m}$ and $\lambda_{k\ell m}$ as the solutions of Rydberg states. Instead we use the $F_{k\ell m}$ functions as basis functions. We expect these functions to outperform most other arbitrarily chosen basis functions.

B. Diagonalization

From Eqs. (2)-(5), we have a system of equations for the coefficients $c_{k\ell}$ in Eq. (4),

$$(H - \epsilon S)_{\mu\nu} c_{\nu} = 0, \quad (10)$$

with the matrix elements

$$H_{k\ell m, k'\ell'm} = -\frac{1}{2} \int dr F_{k\ell m}(r) \left[\frac{d^2}{dr^2} - \frac{\ell(\ell+1)}{r^2} - V_{\ell m, \ell'm}(r) - W_{\ell m, \ell'm}(r) \right] F_{k'\ell'm}(r), \quad (11)$$

$$S_{k\ell m, k'\ell'm} = \int F_{k\ell m}^*(r) Y_{\ell m}^*(\hat{r}) F_{k'\ell'm}(r) Y_{\ell'm}(\hat{r}) dr d\hat{r}. \quad (12)$$

Because we used the frozen-core approximation, c obtained from Eq. (10) does not yield wave functions that are orthogonal to the occupied orbitals. To ensure the orthogonality we make the following modification. For example, in the case of Σ states, we construct a new set of orthogonal basis functions by using the c 's obtained from Eq. (10), i.e.,

$$\chi_v(\sigma_g) = \sum_{k\ell} c_{k\ell, v} u_{k\ell m} + \sum_i a_{i, v} \phi_i(\sigma_g), \quad v = 1, 2, \dots, \quad (13)$$

where $\phi_i(\sigma_g)$ are the three occupied orbitals ($1\sigma_g$, $2\sigma_g$, $3\sigma_g$), and the index v indicates the collating sequence of eigenvalues. The χ functions are then used as basis to construct the Hamiltonian and overlap matrices H' and S' .

Solution of new secular equation

$$(H' - \epsilon' S') b = 0, \quad (14)$$

gives the orthogonalized Rydberg functions, e.g.,

$$\psi_\mu(\sigma_g) = \sum_v b_{v, \mu} \chi_v(\sigma_g) = \sum_{k\ell} c'_{k\ell, \mu} u_{k\ell m}(r) + \sum_i a'_{i, \mu} \phi_i(\sigma_g), \quad \mu = 1, 2, \dots \quad (15)$$

We have solved eight different sets of secular equations corresponding to the $1,3\Sigma_g^+$, $1,3\Sigma_u^+$, $1,3\Pi_g$, and $1,3\Pi_u$ states. The MO ϕ_i in Eq. (15) are drawn from the occupied orbitals, ($1\sigma_g$), ($2\sigma_g$), ($3\sigma_g$), ($1\sigma_u$), ($1\pi_u$) according to the symmetry of each secular equation. The eigenvalues obtained from Eq. (14) are shown in Tables VI - XIII. Here, as in Tables II-V, we present six digits for the eigenvalues in order to see how closely the ϵ' -eigenvalues approach the λ -eigenvalues and the hydrogenic levels with increasing ℓ .

A. The $\lambda_{k\ell m}$ eigenvalues

Inasmuch as the λ eigenvalues in Eq. (6) for large k may be taken as the first approximation to the energy levels of the Rydberg states, it is instructive to analyze the values of λ in terms of the effective potentials V and W in Eq. (6). The index k specifies the number of nodes of $F_{k\ell m}(r)$ which is equal to $k-\ell-1$. The values of λ shown in Table II-V reveal the following features in comparison with the energy levels of the H atom which are included in the last column of Table IV:

- (1) The values of $\lambda_{k\ell m}$ with $\ell \geq 4$ are very close to the corresponding hydrogenic levels, suggesting that these basis functions may already be a fair representation of the respective states.
- (2) The values of $\lambda_{k\ell m}$ with $\ell = 0, 1, 2$ show no resemblance to the corresponding hydrogenic levels.
- (3) For $\ell = 3$ the λ -values of the $(kf)^1\Sigma_u^+$ ($\ell = 3$) series appear to be displaced nearly by one unit in k from the hydrogenic levels, whereas the members of the $(kf)^1\Pi_u$ series are close to the hydrogenic levels of the same k .

The finite separation of the nuclei is an obvious cause of departure from the central field. Figs. 1-3 illustrate the difference

$$\Delta V_{\ell m, \ell m} = V_{\ell m, \ell m} - (-1/r). \quad (16)$$

Because of the strong attraction by the nuclei, ΔV shows a potential cusp at the nuclear site ($r_N = R/2 = 1.05 a_0$). ΔV is negative for $r > 0.3 a_0$. It covers a range of $r \approx 0.6 - 1.5 a_0$ and becomes negligible at $r \approx 2.0 a_0$. The position of the cusp is evidently dictated by the geometry of the molecular ion, but the depth of V depends

not only on the core orbitals but also on the symmetry (l, m) of the Rydberg state under consideration. For instance σ -type Rydberg orbitals in general overlap more favorably with the charge density of the N_2^+ core than do π -type Rydberg orbitals. This is reflected by the larger $|\Delta V|$ for the Σ states since all the Rydberg states considered in this paper have a common $N_2^+ ({}^2\Sigma_g^+)$ core. The attractive perturbation ΔV must be weighed against the repulsive centrifugal term $l(l+1)/r^2$ in Eq. (6). For $l \geq 4$ the centrifugal barrier completely overpowers ΔV and keeps the F_{klm} functions so far away from the origin that they have virtually no overlap with ΔV . The corresponding λ 's should be very close to the hydrogen value of $-\frac{1}{2}k^2$. For smaller l the perturbation ΔV shifts the nodal points of $F_{klm}(r)$ relative to the corresponding hydrogenic wave functions as discussed in Refs. 6 and 13. Moreover the strongly attractive potential well of V has a number of deep bound states which correspond roughly to the core orbitals of N_2 . These deep bound orbitals add further complexities to the nodal structure of the Rydberg orbitals through the orthogonality requirement. Hence we find a wide range of shift of λ_{klm} from the hydrogen limit $-\frac{1}{2}k^2$ for $l \leq 3$.

The effect of electron exchange may be estimated perturbatively by using the hydrogen radial function R_{nl} ; namely, we have computed

$$\overline{\Delta V}_{klm} = \int R_{kl}^2(r) \Delta V_{lm, lm}(r) r^2 dr, \quad (17)$$

and

$$\overline{W}_{klm} = \int R_{kl}^2(r) W_{lm, lm}(r) r^2 dr. \quad (18)$$

For the $(ks) {}^1\Sigma_g^+$ series the ratio $|\overline{W}/\overline{\Delta V}|$ ranges from 0.049 ($k=4$) to 0.018 ($k=11$); for $(kd) {}^1\Sigma_g^+$, from 0.0047 ($k=4$) to 0.0021 ($k=11$); for $(kp) {}^1\Sigma_u^+$,

from 0.15 ($k=4$) to 0.061 ($k=11$); for $(kd)^1\Pi_g$, from 0.0063 ($k=4$) to 0.0029 ($k=11$); and for $(kp)^1\Pi_u$, from 0.14 ($k=4$) to 0.052 ($k=11$). For the higher-angular momentum states, the electron exchange is quite negligible (10^{-5} or less).

B. The Rydberg Levels

The energy levels of the Rydberg states are obtained from Eq. (14). Due to the orthogonality requirement, the energy roots associated with the deep levels of the effective potential are eliminated. Equation (14) allows various $(k\ell)$ members to mix within a symmetry of Λ (or m since the N_2^+ core is in a $^2\Sigma_g^+$ state). Except for a few cases there is always a dominant $(k\ell)$ member in each Rydberg state wave function. Thus we label a Rydberg state by n which is taken as the k -value of the dominant member. We also retain the label ℓ even though it is not strictly a good quantum number. The Rydberg state energies are summarized in Tables VI - XIII. By far the strongest mixings occur in the $(ns)^1,3\Sigma_g^+$ and $(nd)^1,3\Sigma_g^+$ series and the mixing coefficients for the singlet states are shown in Tables XIV and XV. Admixture with $(k\ell)$ members of $\ell \geq 4$ are much smaller and omitted from these tables. For the $(ns)^1\Sigma_g^+$ series the identity of n is not clear until we reach $n = 7$. We simply assign $n = 6, 5, \dots$ to the lower roots of the series consecutively. The next group of series shows an appreciable mixing with the adjacent k values but no mixing with the different ℓ values. This group includes the $(np)^1,3\Sigma_u^+$, $(nd)^1,3\Pi_g$, and $(np)^1,3\Pi_u$ states. For illustration abbreviated tables are presented of the singlet states of this group. The mixing coefficients with different $\ell' = \ell \pm 2$ are at most 0.011, and usually much less. The rest of the states ($\ell \geq 4$) are entirely atomic in character with the dominant coefficients $c_{k\ell} \geq 0.9999$. A comparison of the λ -eigenvalues in Tables II - V and with the corresponding ϵ^* -eigenvalues in Tables VI - XIII also confirms this.

The mixing patterns for the triplet states are qualitatively similar to those of the singlet counterparts and are not given here.

We now interpret the energy levels in Tables VI - XIII in terms of the quantum defect δ_{nl} ,

$$E_{nl} = - \frac{1}{2(n-\delta_{nl})^2} . \quad (19)$$

The m -dependence is implied through the symmetry of Rydberg states. Many theoretical analyses have been made on the quantum defect of atomic Rydberg states.¹⁴ Characteristically the quantum defects of an atom depend on l , but are nearly constant of n within an l -series. Further, if l_{\max} is the largest of the angular momenta of the core orbitals, the quantum defect is very small for those Rydberg states of $l > l_{\max}$.

Although a general analogy to the atomic case clearly exists, such a simple characterization of the molecular Rydberg states must be tempered with caution. In the present problem of N_2 , the quantum defect δ_{nl} clearly shows an l -dependence as in the atomic case. But, in contrast to the atomic case, δ_{nl} varies considerably with n . The largest variation of δ_{nl} with n is found with the $(ns)^1\Sigma_g^+$ series in which δ_{nl} varies from 0.718 ($n=4$) to 0.413 ($n=11$); $(nd)^1\Pi_g$, 0.871 ($n=4$) to 0.641 ($n=11$); and $(np)^1\Sigma_u^+$, 1.581 ($n=4$) to 1.309 ($n=11$). These states are characterized by strong mixing of the basis functions as shown in Tables XIV, XVI and XVII. The next group shows a moderate variation, which includes $(np)^1\Pi_u$ for which δ_{nl} ranges from 0.660 ($n=3$) to 0.596 ($n=11$); and $(nd)^1\Sigma_g^+$, 1.0449 ($n=4$) to 1.0325 ($n=11$); and $(nf)^1\Sigma_u^+$, 1.00678 ($n=5$) to 1.00916 ($n=11$). These states have relatively small mixing among the basis functions. In the case of the $(nd)^1\Sigma_g^+$ series an appreciable mixing is found between the basis functions of the (k,d) and $(k-1,s)$ series (see Table XV), but

energetically those two groups of basis functions are very similar. Other states of large l show markedly smaller quantum defects. This is in accord with the concept of penetrating/nonpenetrating atomic orbitals.⁶ [The core orbitals may be decomposed into the constituent l -components. From this analysis, the charge densities are found to be mainly confined to $l \leq 3$: $1\sigma_g$ (42.6%), $2\sigma_g$ (92.5%), $3\sigma_g$ (94.8%), $1\sigma_u$ (60.0%) $2\sigma_u$ (96.9%) $1\pi_u$ (98.0%).] However, even when the quantum defect is small, δ_{nl} is still not entirely constant within a series. A very similar situation exists with the triplet states studied in this paper. Thus, we are not able to support the qualitative prediction¹⁵ that δ_{nl} is constant of n for the N_2 molecule. Since the exact solutions of H_2^+ are available, Mulliken¹⁶ analyzed the quantum defect of H_2^+ as a function of the internuclear separation. At $R = 2.0 a_0$ a comparable variation of δ_{nl} with n is found in H_2^+ . This is consistent with the present results. Moreover, the R -dependence of δ_{nl} may be understood in terms of the combined effect of the angular momentum barrier and the potential cusp $\Delta V(r)$ at $r_N = R/2$. Unfortunately, because of this complexity a generalization of the quantitative features is difficult for molecules.

The $(nd)1\Sigma_g^+$ and $(nf)1\Sigma_u^+$ series have a quantum defect slightly larger than one. If we shift the n scale by one unit, these two series would appear to have very small quantum defects. The same shift would make the apparent quantum defects of $(np)1\Sigma_u^+$ smaller and those of $(nd)1\Pi_g$ negative. Care should be taken to allow for this possible ambiguity in the assignment of n when comparing theoretical Rydberg levels with experiments.

The Rydberg states of N_2 are important to the optical properties of the atmosphere as transitions among many of these states are in the infrared region. Application of the selection rules $\Delta l = \pm 1$, $\Delta \Lambda = 0$ and ± 1 , and $\Delta S = 0$ to the Rydberg levels reported in Tables VI - XIII

yields a vast number of transitions of wavelength in the range of 4-20 μm which are displayed in Figs. 4 and 5. All transitions are drawn to the same height and no consideration was given to their relative intensities. Since we have considered only levels through $n = 11$, Figs. 4 and 5 do not represent a complete listing of all possible transitions in the 4-20 μm region. To illustrate the richness of the Rydberg spectrum we mark in these figures the wavelengths of the limiting hydrogenic transitions of the Rydberg levels involved. Figures 4 and 5 are based on consideration of electronic states with no reference to molecular vibration and rotation. The vibrational potential curves of all the Rydberg states considered here have virtually the same shape as the potential curve of their parent $\text{N}_2^+ (^2\Sigma_g^+)$ state and therefore have identical vibrational frequency. Furthermore the vibrational-level selection rule for electronic transitions between such Rydberg states is $\Delta v = 0$ according to the Franck-Condon principles. Thus the vibrational levels have no effect on the transition frequencies. The rotational levels do produce fine structures in the electronic transitions replacing each line in Figs. 4 and 5 by a band.

IV. COMPARISON WITH OTHER WORKS

The energy levels of those Rydberg states, which may be compared with other works, are compiled in Table XIX. In accordance with the previous works¹ the energy levels are converted to show the term values above the $N_2(X^1\Sigma_g^+)$ ground state based on the fact that $N_2^+(X^2\Sigma_g^+)$ is 15.581 eV above $N_2(X^1\Sigma_g^+)$.

The theoretical calculations of Lefebvre-Brion and Moser⁴ are similar to the present work. Both calculations are quite rigorous within the framework of the frozen-core approximation. In describing the Rydberg orbitals, however, they approached it from the separate-atom picture, whereas we use the united-atom picture as the starting point. Therefore, the reliability of the present work increases with the increasing quantum numbers. The model potential employed in the calculation of Ref. 3 does not reflect the details of the potential of the one-electron Hamiltonian discussed in the previous section. Although the model-potential approach affords a great deal of computational simplicity, it does not include the provision of distinguishing the ionic states ($X^2\Sigma_g^+$, $A^2\Pi_u$, $B^2\Sigma_u^+$) to which the Rydberg states converge, or the spin multiplicity (singlet or triplet) of the Rydberg states. Nevertheless, all three sets of theoretical calculations agree reasonably well.

The experimental data are summarized in the extensive review article by Lofthus and Krupenie.¹ In some cases the experimental values cited in Table XIX are taken from the original papers^{17,18} as annotated. A general agreement is seen between the theory and experiment. Some refinements¹⁹ of the experimental work have been published recently. The new data agree with the earlier ones to within typically five digits. This is below the estimated uncertainty of our theoretical values.

Most of the observed Rydberg levels are confined to the $(np)^1\Sigma_u^+$ and $(np)^1\Pi_u$ series. Since the $3\sigma_g$ orbital has 52% ($l=0$) and 43% ($l=2$) components, it would seem that $(nf)^1\Sigma_u^+$ and $(nf)^1\Pi_u$ states may appear in the absorption spectra analogously to the $(np)^1\Sigma_u^+$ and $(np)^1\Pi_u$ states. However, no experimental evidence has been found so far as to their existence or identity. In this connection we may mention the recent identification of the $k^1\Pi_g$ state as a Rydberg state converging to the $X^2\Sigma_g^+(N_2^+)$.¹⁸ The term value 14.100 eV is close to 14.191 eV of the present calculation.

V. SUMMARY AND CONCLUSIONS

The spectrum of the N_2 molecule is indeed extremely complex. In this paper we have dealt with the electronic part of the problem. We have placed the emphasis on the calculation of high Rydberg states, therefore, the united-atom approach is a natural choice. For high-angular-momentum states the molecular core may be treated as a quasi-spherical one. For low-angular momentum states, mixing of the eigenstates of the limiting quasi-spherical system is necessary. The agreement with other theoretical calculations and experiment is reasonable and satisfactory.

The finite separation of the nuclei adds a new dimension to the problem that is not present in an atomic case. It appears that the properties of Rydberg series may vary greatly from one molecule to another and from one series to another within the same molecule. A rough estimate of the electron-exchange effect is about 15% of the Coulomb effect or less. In the frozen-core approximation adopted here, we take the core orbitals as those of the $N_2^+ (X^2\Sigma_g^+)$ ion and neglect any orbital readjustment due to the addition of the Rydberg electron. Such a charge redistribution is often referred to as the core polarization which is sometimes treated by introducing the polarization potential $-\alpha/2r^4$ where α is the polarizability. For the case of atoms, Van Vleck and Whitelaw²⁰ have shown that the use of the polarization potential is valid only under several restrictive conditions. To fully address this point and other pertinent questions such as electron-correlation energy would require computations on the level of configuration interaction. Although the multiconfiguration self-consistent-field method has been applied to the ground and low excited states of molecules, it would be an enormous undertaking to incorporate the multiconfiguration scheme to the Rydberg states. At this time a more practical direction to improve

the present work is to allow the core orbitals to relax under the influence of the Rydberg electron. The core-orbital relaxation should be more important for the lower Rydberg states. This is consistent with our observation that the lower Rydberg states show larger discrepancy between theory and experiment in Table XIX. Furthermore inclusion of core-orbital relaxation by a variational procedure would lower the calculated Rydberg levels making a change in the right direction toward the experimental values.

REFERENCES

1. A. Lofthus and P. H. Krupenie, *J. Phys. and Chem. Ref. Data*, 6, 113 (1977).
2. A. B. F. Duncan, *J. Chem. Phys.* 42, 2453 (1965); A. B. F. Duncan and A. Damiani, *J. Chem. Phys.* 45, 1245 (1966).
3. T. Betts and V. McKoy, *J. Chem. Phys.* 54, 113 (1971).
4. H. Lefebvre-Brion and C. M. Moser, *J. Chem. Phys.* 43, 1394 (1965).
5. A. U. Hazi and S. A. Rice, *J. Chem. Phys.* 48, 495 (1968); J. D. Weeks, A. Hazi, and S. A. Rice, *Adv. Chem. Phys.* 16, 283 (1969).
6. R. S. Mulliken, *J. Am. Chem. Soc.* 86, 3183 (1964); 88, 1849 (1966).
7. K. Dressler, *Can. J. Phys.* 47, 547 (1969); P. K. Carroll and C. P. Collins, *Can. J. Phys.* 47, 563 (1969).
8. C. C. J. Roothaan, *Rev. Mod. Phys.* 23, 69 (1951); 32, 179 (1960).
9. T. K. Holley, S. Chung, C. C. Lin, and E. T. P. Lee, *Phys. Rev. A* 24, 2946 (1981), Table I.
10. S. Chung and C. C. Lin, *Phys. Rev. A* 17, 1874 (1978).
11. F. Herman and S. Skillman, Atomic Structure Calculations (Prentice-Hall, Englewood Cliffs, N.J., 1963).
12. W. D. Robb, and L. A. Collins, *Bull. Am. Phys. Soc.* 24, 1170 (1979).
13. M. Kotani, in Molecular Orbitals in Chemistry, Physics and Biology, P. O. Lowdin and B. Pullman (eds.) (Academic Press, New York, 1964), p. 539.
14. See, for example, R. R. Freeman and D. Kleppner, *Phys. Rev. A* 14, 1614 (1976); T. N. Chang and R. T. Poe, *Phys. Rev. A* 10, 1981 (1974).
15. E. Lindholm, *Arkiv Fys.* 40, 111 (1969).

16. See, Sec. V of Ref. 6, and the tables therein.
17. P. K. Carroll and K. Yoshino, J. Phys. B 5, 1614 (1972); P. K. Carroll, J. Chem. Phys. 58, 3597 (1973).
18. P. K. Carroll and K. V. Subbaram, Can. J. Phys., 53, 2198 (1975).
19. See, for example, T. Suzuki and M. Kakimoto, J. Mol. Spectrosc. 93, 423 (1982); K. Yoshino, D. E. Freeman, and Y. Tanaka, J. Mol. Spectrosc. 76, 153 (1979).
20. J. H. Van Vleck and N. G. Whitelaw, Phys. Rev. 44, 551 (1933).

Table I. Mesh size of integration^a in a_0 .

r_1	δr	r_f
0.0	0.0125	1.5
1.5	0.0250	2.5
2.5	0.0500	5.5
5.5	0.1000	12.5
12.5	0.2000	356.5

^a r_1 and r_f are the starting and terminating points respectively with the step-size δr .

Table II. λ -eigenvalues of $^1\Sigma_g^+(m = 0)$ type basis functions^a.

k	$l = 0$	$l = 2$	$l = 4$	$l = 6$	$l = 8$
1	-2.92183(0) ^b				
2	-1.59652(-1)				
3	-6.55096(-2)	-2.21840(0)			
4	-3.53493(-2)	-5.60753(-2)			
5	-2.20659(-2)	-3.14138(-2)	-2.00297(-2)		
6	-1.50711(-2)	-2.00714(-2)	-1.39061(-2)		
7	-1.09426(-2)	-1.39264(-2)	-1.02149(-2)	-1.02075(-2)	
8	-8.30418(-3)	-1.02263(-2)	-7.81968(-3)	-7.81472(-3)	
9	-6.51646(-3)	-7.82672(-3)	-6.17785(-3)	-6.17435(-3)	-6.17345(-3)
10	-5.24949(-3)	-6.18248(-3)	-5.00361(-3)	-5.00107(-3)	-5.00039(-3)
11	-4.31904(-3)	-5.00684(-3)	-4.13492(-3)	-4.13300(-3)	-4.13249(-3)

^aIn atomic units (1 a.u. = 27.21 eV).

^bNumbers inside parentheses indicate the power of 10.

Table III. λ -eigenvalues of $1\Sigma_u^+$ ($m = 0$) type basis functions^a.

k	$\ell = 1$	$\ell = 3$	$\ell = 5$	$\ell = 7$	$\ell = 9$
2	-3.53198(0)				
3	-1.95374(-1)				
4	-6.52276(-2)	-2.25576(-1)			
5	-3.46552(-2)	-3.13678(-2)			
6	-2.16090(-2)	-2.00570(-2)	-1.38980(-2)		
7	-1.47799(-2)	-1.39207(-2)	-1.02098(-2)		
8	-1.07502(-2)	-1.02236(-2)	-7.81628(-3)	-7.81390(-3)	
9	-8.17186(-3)	-7.82535(-3)	-6.17545(-3)	-6.17377(-3)	
10	-6.42207(-3)	-6.18174(-3)	-5.00188(-3)	-5.00063(-3)	-5.00027(-3)
11	-5.17998(-3)	-5.00639(-3)	-4.13359(-3)	-4.13268(-3)	-4.13239(-3)

^aSee the footnotes in Table II.

Table IV. λ -eigenvalues of $^1\Pi_g$ ($m = 1$) type basis functions^a.

k	$l = 2$	$l = 4$	$l = 6$	$l = 8$	Hydrogenic ^b
3	-6.74709(-2)				-5.55556(-2)
4	-3.84349(-2)				-3.12500(-2)
5	-2.39647(-2)	-2.00253(-2)			-2.00000(-2)
6	-1.62267(-2)	-1.39034(-2)			-1.38889(-2)
7	-1.16817(-2)	-1.02132(-2)	-1.02072(-2)		-1.02041(-2)
8	-8.80125(-3)	-7.81856(-3)	-7.81455(-3)		-7.81250(-3)
9	-6.86535(-3)	-6.17706(-3)	-6.17424(-3)	-6.17340(-3)	-6.17284(-3)
10	-5.50324(-3)	-5.00304(-3)	-5.00098(-3)	-5.00037(-3)	-5.00000(-3)
11	-4.50910(-3)	-4.13448(-3)	-4.13293(-3)	-4.13248(-3)	-4.13223(-3)

^aSee the footnotes in Table II.^bEnergy levels of H atom ($= -1/2k^2$)

Table V. Eigenvalues of $l_{\mu}^{(m-1)}$ type basis functions^a.

k	$l = 1$	$l = 3$	$l = 5$	$l = 7$	$l = 9$
2	-6.63839(-1)				
3	-8.58743(-2)				
4	-4.22486(-2)	-3.13557(-2)			
5	-2.52510(-2)	-2.00572(-2)			
6	-1.68054(-2)	-1.39231(-2)	-1.38971(-2)		
7	-1.19918(-2)	-1.02260(-2)	-1.02092(-2)		
8	-8.98732(-3)	-7.82732(-3)	-7.81590(-3)	-7.81383(-3)	
9	-6.98617(-3)	-6.18330(-3)	-6.17518(-3)	-6.17372(-3)	
10	-5.58631(-3)	-5.00766(-3)	-5.00166(-3)	-5.00059(-3)	-5.00024(-3)
11	-4.56879(-3)	-4.13796(-3)	-4.13346(-3)	-4.13265(-3)	-4.13237(-3)

^aSee the footnotes in Table II.

Table VI. Energy levels of $1\Sigma_g^+$ type Rydberg states^a.

n	$\ell = 0$	$\ell = 2$	$\ell = 4$	$\ell = 6$	$\ell = 8$
3	-1.06273(-1) ^b				
4	-4.64080(-2)	-5.72547(-2)			
5	-2.64274(-2)	-3.19593(-2)	-2.00298(-2)		
6	-1.71486(-2)	-2.03465(-2)	-1.39062(-2)		
7	-1.20559(-2)	-1.40793(-2)	-1.02150(-2)	-1.02078(-2)	
8	-8.94882(-3)	-1.03180(-2)	-7.81987(-3)	-7.81498(-3)	
9	-6.90857(-3)	-7.88498(-3)	-6.17811(-3)	-6.17465(-3)	-6.17376(-3)
10	-5.49274(-3)	-6.22097(-3)	-5.00386(-3)	-5.00134(-3)	-5.00067(-3)
11	-4.46081(-3)	-5.03262(-3)	-4.13517(-3)	-4.13328(-3)	-4.13278(-3)

^a In atomic units (1 a.u. = 27.21 eV) below N_2^+ ($X^2\Sigma_g^+$)

^b Numbers inside parentheses indicate the power of 10.

Table VII. Energy levels of $1\epsilon_u^+$ type Rydberg states^a.

n	$\ell = 1^b$	$\ell = 3$	$\ell = 5$	$\ell = 7$	$\ell = 9$
4	-1.02772(-1)	-8.54582(-2)			
5	-4.18326(-2)	-3.13956(-2)			
6	-2.48972(-2)	-2.00775(-2)	-1.38983(-2)		
7	-1.64735(-2)	-1.39314(-2)	-1.02101(-2)		
8	-1.16248(-2)	-1.02309(-2)	-7.81653(-3)	-7.81419(-3)	
9	-8.53928(-3)	-7.83020(-3)	-6.17575(-3)	-6.17407(-3)	
10	-6.65276(-3)	-6.18573(-3)	-5.00213(-3)	-5.00092(-3)	-5.00056(-3)
11	-5.32418(-3)	-5.00917(-3)	-4.13387(-3)	-4.13296(-3)	-4.13267(-3)

^a See the footnotes in Table VI.

^b The n values are consistent with Mulliken's assignment (Ref. 6), but differ by one unit from Dressler's assignment (Ref. 7).

Table VIII. Energy levels of $1\Pi_g$ type Rydberg states^a.

n	$l = 2$	$l = 4$	$l = 6$	$l = 8$
4	-5.10714(-2)			
5	-2.85280(-2)	-2.00253(-2)		
6	-1.83158(-2)	-1.39036(-2)		
7	-1.27814(-2)	-1.02134(-2)	-1.02075(-2)	
8	-9.43470(-3)	-7.81880(-3)	-7.81484(-3)	
9	-7.25213(-3)	-6.17733(-3)	-6.17453(-3)	-6.17373(-3)
10	-5.74681(-3)	-5.00330(-3)	-5.00126(-3)	-5.00066(-3)
11	-4.65981(-3)	-4.13475(-3)	-4.13322(-3)	-4.13277(-3)

^a See the footnotes in Table VI.

Table IX. Energy levels of $1\Pi_u$ type Rydberg states^a.

n	$l = 1$	$l = 3$	$l = 5$	$l = 7$	$l = 9$
3	-9.13323(-2)				
4	-4.40846(-2)	-3.13501(-2)			
5	-2.60713(-2)	-2.00529(-2)			
6	-1.72373(-2)	-1.39201(-2)	-1.38974(-2)		
7	-1.22442(-2)	-1.02240(-2)	-1.02095(-2)		
8	-9.14621(-3)	-7.82596(-3)	-7.81615(-3)	-7.81411(-3)	
9	-7.09158(-3)	-6.18238(-3)	-6.17547(-3)	-6.17401(-3)	
10	-5.65876(-3)	-5.00700(-3)	-5.00193(-3)	-5.00090(-3)	-5.00054(-3)
11	-4.61911(-3)	-4.13754(-3)	-4.13373(-3)	-4.13293(-3)	-4.13266(-3)

^a See the footnotes in Table VI.

Table X. Energy levels of $^3\Sigma_g^+$ type Rydberg states^a.

n	$l = 0$	$l = 2$	$l = 4$	$l = 6$	$l = 8$
3	-1.13895(-1)				
4	-4.86088(-2)	-5.79860(-2)			
5	-2.73442(-2)	-3.23170(-2)	-2.00298(-2)		
6	-1.75921(-2)	-2.05351(-2)	-1.39063(-2)		
7	-1.22914(-2)	-1.41883(-2)	-1.02151(-2)	-1.02078(-2)	
8	-9.08172(-3)	-1.03858(-2)	-7.81988(-3)	-7.81499(-3)	
9	-6.98621(-3)	-7.92941(-3)	-6.71812(-3)	-6.17465(-3)	-6.17376(-3)
10	-5.53839(-3)	-6.25120(-3)	-5.00386(-3)	-5.00134(-3)	-5.00067(-3)
11	-4.48675(-3)	-5.05343(-3)	-4.13518(-3)	-4.13328(-3)	-4.13278(-3)

^a See the footnotes in Table VI.

Table XI. Energy levels of $^3\Sigma_u^+$ type Rydberg states^a.

n	$l = 1$	$l = 3$	$l = 5$	$l = 7$	$l = 9$
4	-1.03570(-1)	-8.72696(-2)			
5	-4.25219(-2)	-3.14252(-2)			
6	-2.52225(-2)	-2.00996(-2)	-1.38983(-2)		
7	-1.66328(-2)	-1.39399(-2)	-1.02101(-2)		
8	-1.17026(-2)	-1.02361(-2)	-7.81654(-3)	-7.81420(-3)	
9	-8.87308(-3)	-7.83264(-3)	-6.17575(-3)	-6.17407(-3)	
10	-6.66733(-3)	-6.18715(-3)	-5.00214(-3)	-5.00093(-3)	-5.00056(-3)
11	-5.33223(-3)	-5.01050(-3)	-4.13388(-3)	-4.13297(-3)	-4.13267(-3)

^aSee the footnotes in Table VI.

Table XII. Energy levels of $^3\Pi_g$ type Rydberg states^a.

n	$l = 2$	$l = 4$	$l = 6$	$l = 8$
4	-5.16214(-2)			
5	-2.87212(-2)	-2.00254(-2)		
6	-1.84182(-2)	-1.39037(-2)		
7	-1.28411(-2)	-1.02135(-2)	-1.02075(-2)	
8	-9.46553(-3)	-7.81880(-3)	-7.81484(-3)	
9	-7.27266(-3)	-6.17733(-3)	-6.17453(-3)	-6.17371(-3)
10	-5.76093(-3)	-5.00331(-3)	-5.00126(-3)	-5.00066(-3)
11	-4.66932(-3)	-4.13475(-3)	-4.13322(-3)	-4.13277(-3)

^aSee the footnotes in Table VI.

Table XIII. Energy levels of $^3\Pi_u$ type Rydberg states^a.

n	$l = 1$	$l = 3$	$l = 5$	$l = 7$	$l = 9$
		0			
3	-9.19470(-2)				
4	-4.42717(-2)	-3.13516(-2)			
5	-2.61497(-2)	-2.00579(-2)			
6	-1.72766(-2)	-1.39237(-2)	-1.38974(-2)		
7	-1.22662(-2)	-1.02265(-2)	-1.02095(-2)		
8	-9.15955(-3)	-7.82781(-3)	-7.81615(-3)	-7.81411(-3)	
9	-7.10009(-3)	-6.18374(-3)	-6.17548(-3)	-6.17401(-3)	
10	-5.66435(-3)	-5.00803(-3)	-5.00193(-3)	-5.00090(-3)	-5.00054(-3)
11	-4.62274(-3)	-4.13833(-3)	-4.13373(-3)	-4.13293(-3)	-4.13266(-3)

^aSee the footnotes in Table VI.

Table XIV. Mixing coefficients in Eq. (16) for $(ns)^1\Sigma_g^+$ states.

(kℓ)	n = 3	n = 4	n = 5	n = 6	n = 7	n = 8	n = 9	n = 10	n = 11
1s	-0.239	0.130	0.084	-0.058	0.042	0.031	0.023	0.017	-0.011
2s	0.873	-0.239	-0.133	0.087	-0.061	-0.045	-0.034	-0.025	0.018
3s	-0.479	-0.611	-0.196	0.110	-0.073	-0.051	-0.038	-0.028	0.019
4s	-0.162	0.618	-0.506	0.173	-0.098	-0.065	-0.046	-0.033	0.023
5s	-0.093	0.191	0.704	0.437	-0.156	-0.089	-0.059	-0.041	0.027
6s	-0.063	0.110	0.200	-0.763	-0.383	-0.141	-0.081	-0.052	0.034
7s	-0.047	0.075	0.114	-0.199	0.808	-0.338	-0.127	-0.071	0.043
8s	-0.037	0.057	0.079	-0.113	0.194	0.845	-0.297	-0.112	0.058
9s	-0.030	0.045	0.056	-0.078	0.109	0.186	0.877	-0.255	0.091
10s	-0.025	0.037	0.047	-0.059	0.075	0.104	0.176	0.910	0.200
11s	-0.022	0.031	0.039	-0.047	0.057	0.071	0.097	0.162	-0.963
3d	-0.269	-0.019	0.013	0.009	0.007	0.005	0.004	0.003	-0.003
4d	-0.096	-0.337	-0.073	0.039	-0.025	-0.018	-0.013	-0.009	0.006
5d	-0.047	0.146	-0.300	0.074	-0.040	-0.026	-0.018	-0.013	0.009
6d	-0.031	0.061	0.169	0.262	-0.070	-0.038	-0.024	-0.017	0.011
7d	-0.022	0.038	0.066	-0.180	-0.229	-0.064	-0.035	-0.022	0.014
8d	-0.017	0.027	0.041	-0.067	0.185	-0.200	-0.058	-0.031	0.018
9d	-0.014	0.021	0.029	-0.041	0.066	0.186	-0.173	-0.052	0.025
10d	-0.011	0.017	0.023	-0.029	0.040	0.063	0.183	-0.146	0.041
11d	-0.010	0.014	0.018	-0.023	0.028	0.038	0.060	0.177	0.111
1 σ_g	0.070	-0.039	-0.026	0.018	-0.013	-0.010	-0.007	-0.005	0.004
2 σ_g	0.256	-0.138	-0.089	0.061	0.044	-0.033	-0.024	-0.018	0.011
3 σ_g	0.194	-0.110	0.072	0.050	-0.036	-0.027	-0.021	-0.016	0.011

Table XV. Mixing coefficients in Eq. (16) for $(nd)^1 + g$ states.

(kl)	n = 4	n = 5	n = 6	n = 7	n = 8	n = 9	n = 10	n = 11
1s	0.084	0.058	0.042	0.032	-0.025	0.020	-0.016	0.013
2s	-0.086	-0.045	-0.028	0.020	-0.014	-0.011	0.009	-0.007
3s	-0.369	-0.066	-0.035	-0.022	0.016	-0.012	0.009	-0.007
4s	0.083	-0.356	-0.058	-0.030	0.019	-0.014	0.010	-0.008
5s	0.035	0.084	-0.333	-0.053	0.027	-0.018	0.012	-0.009
6s	0.022	0.036	0.081	-0.310	0.049	-0.025	0.016	-0.011
7s	0.015	0.023	0.035	0.077	0.289	-0.046	0.023	-0.014
8s	0.012	0.016	0.022	0.034	-0.073	-0.269	0.042	-0.021
9s	0.009	0.013	0.016	0.021	-0.032	0.069	0.247	-0.038
10s	0.008	0.010	0.013	0.016	-0.020	0.030	-0.064	-0.221
11s	0.007	0.008	0.010	0.012	-0.015	0.019	-0.028	0.058
3d	-0.009	-0.007	-0.005	-0.004	0.004	-0.003	0.003	-0.002
4d	0.921	-0.030	-0.014	-0.009	0.006	-0.005	0.003	-0.003
5d	0.027	0.925	-0.032	-0.015	0.009	-0.006	0.005	-0.004
6d	0.014	0.030	0.934	-0.031	0.015	-0.009	0.006	-0.005
7d	0.009	0.015	0.030	0.943	0.030	-0.014	0.009	-0.006
8d	0.006	0.010	0.015	0.029	-0.950	-0.029	0.013	-0.008
9d	0.005	0.007	0.010	0.015	-0.028	0.957	0.027	-0.012
10d	0.004	0.006	0.007	0.010	-0.014	0.027	-0.964	-0.025
11d	0.003	0.005	0.006	0.007	-0.010	0.014	-0.026	0.972
1 σ_g	-0.019	-0.013	0.009	-0.007	0.005	-0.004	0.003	-0.003
2 σ_g	-0.088	-0.061	-0.044	-0.033	0.026	-0.020	0.017	-0.014
3 σ_g	-0.022	-0.013	-0.009	-0.006	0.004	-0.003	0.002	-0.002

Table XVI. Mixing Coefficients in Eq. (16) for $(np)^1\Sigma_u^+$ states.

	$k = n-2$	$k = n-1$	$k = n$	$k = n+1$
$n = 4^a$	-0.071	0.491	-0.857	-0.169
$n = 5$	-0.206	-0.315	0.905	-0.170
$n = 6$	-0.125	-0.269	0.927	0.163
$n = 7$	0.109	0.240	-0.940	-0.155
$n = 8$	-0.098	-0.217	0.951	0.147
$n = 9$	-0.090	-0.197	0.960	-0.138
$n = 10$	0.081	0.177	-0.969	-0.128
$n = 11$	-0.070	-0.152	0.983	

^a
 $\ell = 1$ in all basis functions (k, ℓ) .

Table XVII. Mixing coefficients in Eq. (16) for $(nd)^1\Pi_g$ states.

	$k = n-2$	$k = n-1$	$k = n$	$k = n+1$
$n = 4^a$		-0.749	0.624	0.189
$n = 5$	-0.216	-0.545	0.770	0.203
$n = 6$	-0.188	-0.435	0.837	0.200
$n = 7$	0.159	0.368	-0.875	-0.192
$n = 8$	-0.140	-0.321	0.902	0.182
$n = 9$	-0.124	-0.281	0.924	0.171
$n = 10$	-0.109	-0.245	0.944	0.159
$n = 11$	0.092	0.202	-0.970	

^a $\ell = 2$ in all basis functions (k, ℓ)

Table XVIII. Mixing coefficients in Eq. (16) for $(np)^1\Pi_u$ states.

	$k = n-2$	$k = n-1$	$k = n$	$k = n+1$
$n = 3^a$		-0.177	0.988	0.063
$n = 4$	-0.097	-0.076	0.991	0.065
$n = 5$	0.035	0.075	-0.992	-0.062
$n = 6$	-0.035	-0.073	0.993	0.063
$n = 7$	-0.034	-0.071	0.993	0.062
$n = 8$	0.033	0.069	-0.994	-0.060
$n = 9$	0.032	0.067	-0.994	-0.059
$n = 10$	-0.031	-0.064	0.995	0.057
$n = 11$	-0.029	-0.060	0.997	

^a $\ell = 1$ in all basis functions (k, ℓ) .

	Present	Ref. 4	Ref. 3 ^b	Experiment
(np) $1\Sigma_u^+$	n=4 12.785	13.1	12.98	12.935 ^c
	5 14.443	14.4	14.35	14.364
	6 14.904	14.9	14.86	14.871
	7 15.133		15.13	15.110
	8 15.265			15.245
	9 15.349			15.332
	10 15.400			15.386
	11 15.436			15.426
(np) $1\Pi_u$	n=3 13.096	13.1	12.95	12.982 ^c
	4 14.381	14.5	14.32	14.329
	5 14.872	15.0	14.81	14.846
	6 15.112		15.11	15.098
	7 15.248			15.238
	8 15.332			15.327
	9 15.388			15.385
	10 15.427			15.425
	11 15.455			15.454
(ns) $1\Sigma_g^+$	n=3 ^d 12.689	12.5		12.25 ^e
	4 14.318	14.0		
(nd) $1\Pi_g$	n=4 14.191		13.06	14.100 ^f
(np) $3\Sigma_u^+$	n=4 ^g 12.763	13.0		12.84 ^f
	5 14.424	14.4		
	6 14.895	14.9		
(np) $3\Pi_u$	n=3 13.079	13.0		12.8 ^e
	4 14.376	14.4		
	5 14.869	14.9		
(ns) $3\Sigma_g^+$	n=3 ^h 12.482	11.9		11.87 ^e
	4 14.258	13.9		

^a Measured in eV above $N_2(X^1\Sigma_g^+)$; See text.

^b Singlet-triplet distinction cannot be made; see text.

^c Ref. 17.

^d $a''^1\Sigma_g^+$.

^e Ref. 1.

^f Ref. 18.

^g $D^3\Sigma_u^+$.

^h $E^3\Sigma_g^+$.

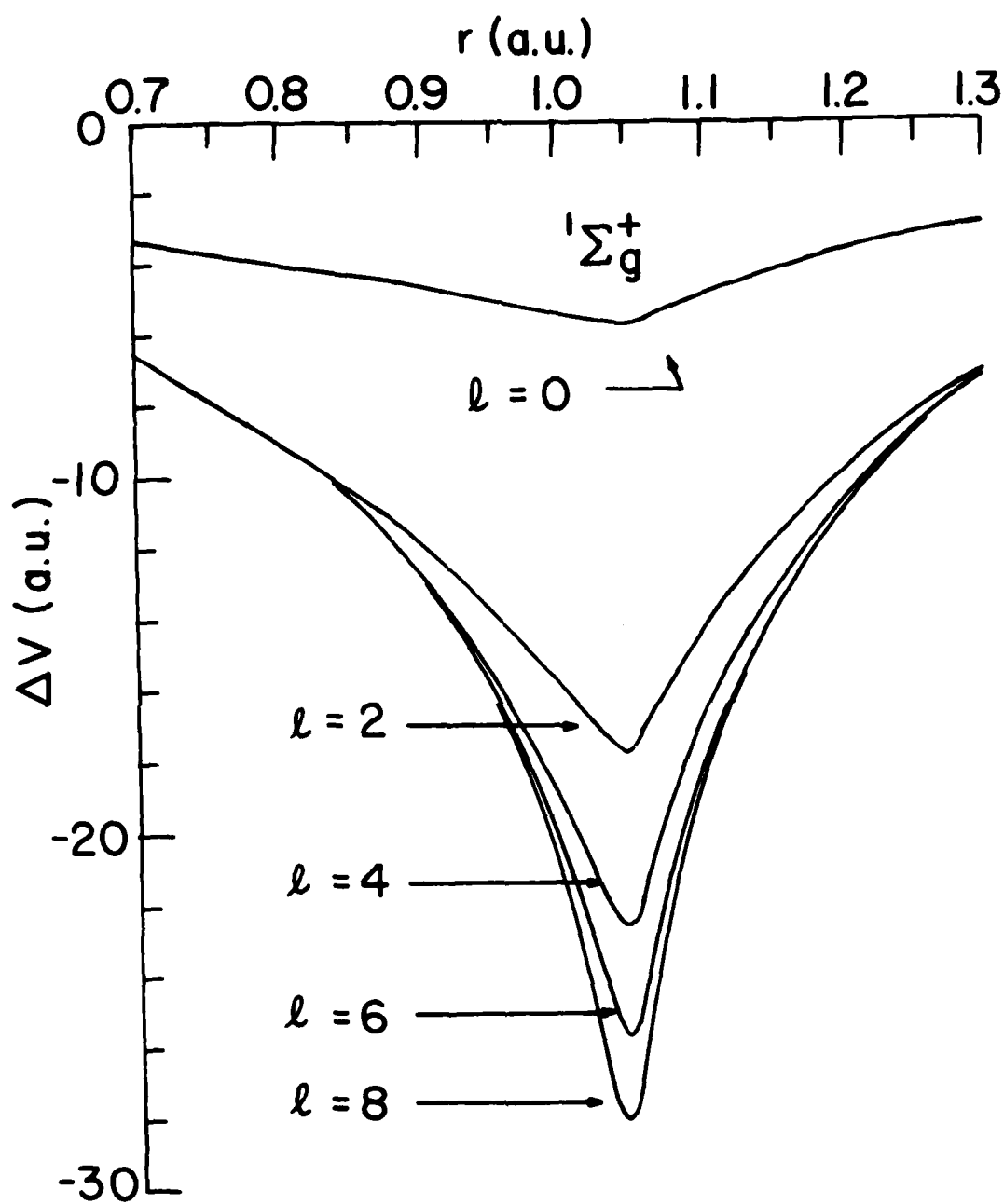


Figure 1. Plots of ΔV in Eq. (16) versus r for the $1\Sigma_g^+$ symmetry.

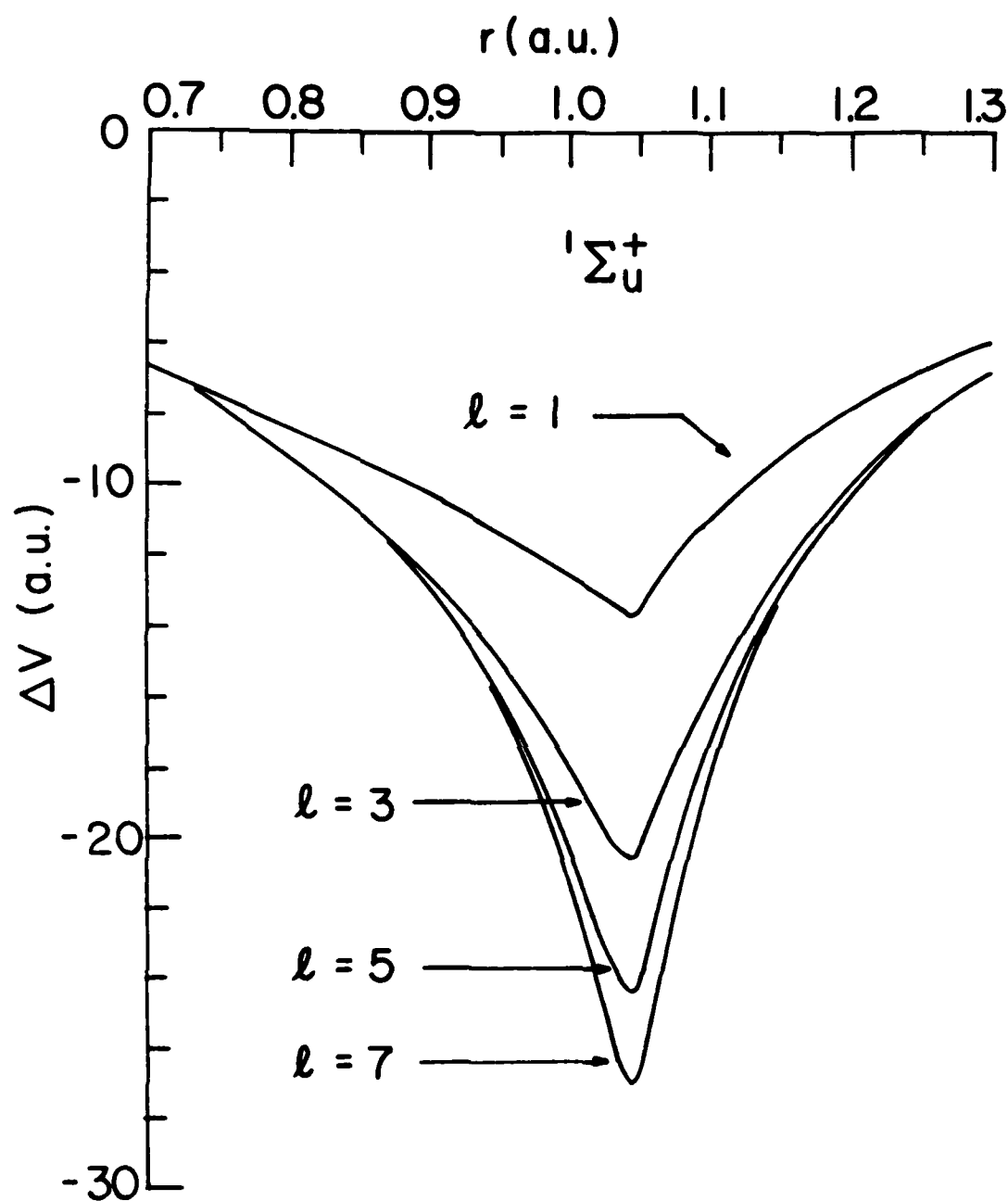


Figure 2. Plots of ΔV in Eq. (16) versus r for the $1\Sigma_u^+$ symmetry.

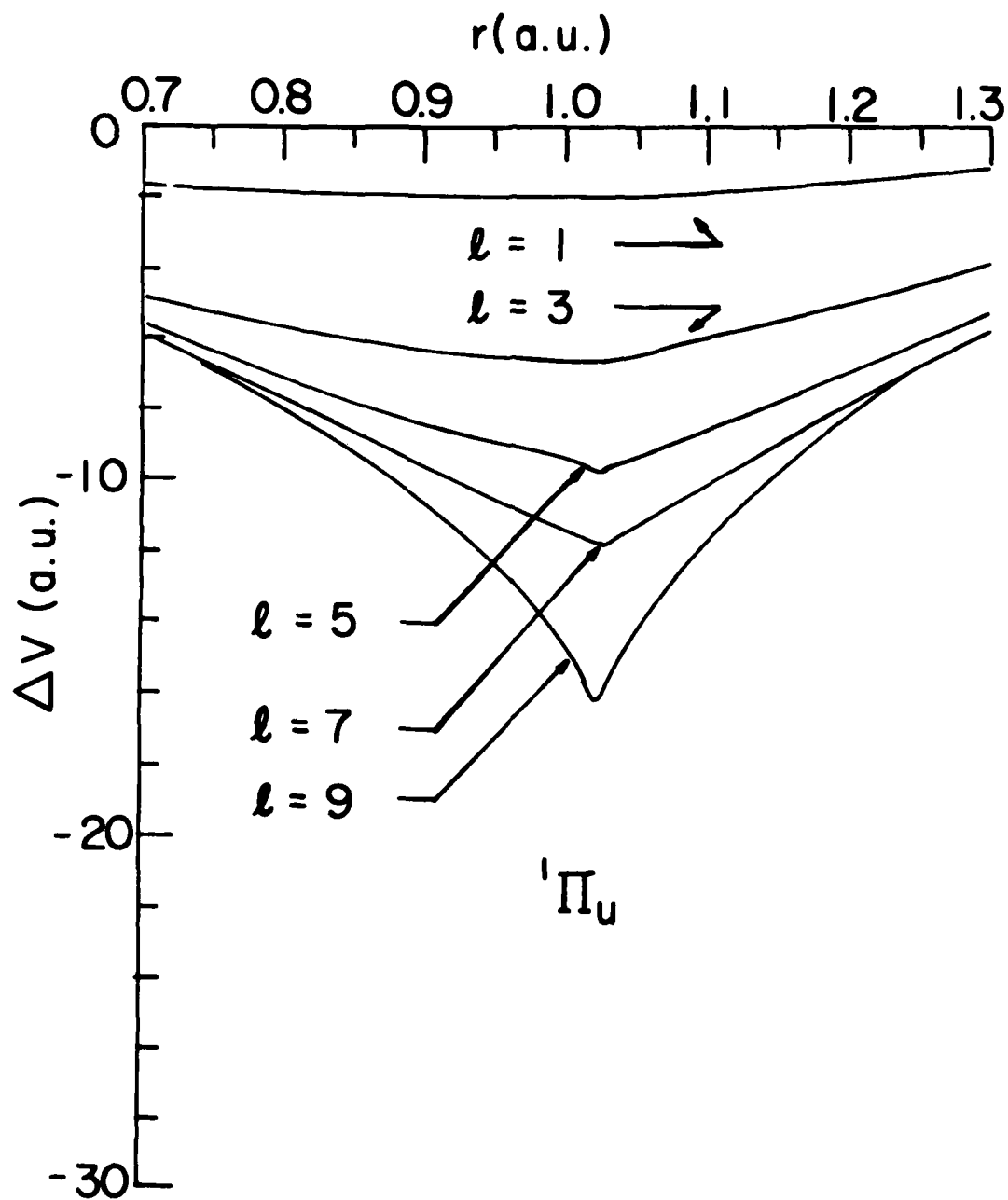


Figure 3. Plots of ΔV in Eq. (16) versus r for the ${}^1\Pi_u$ symmetry.

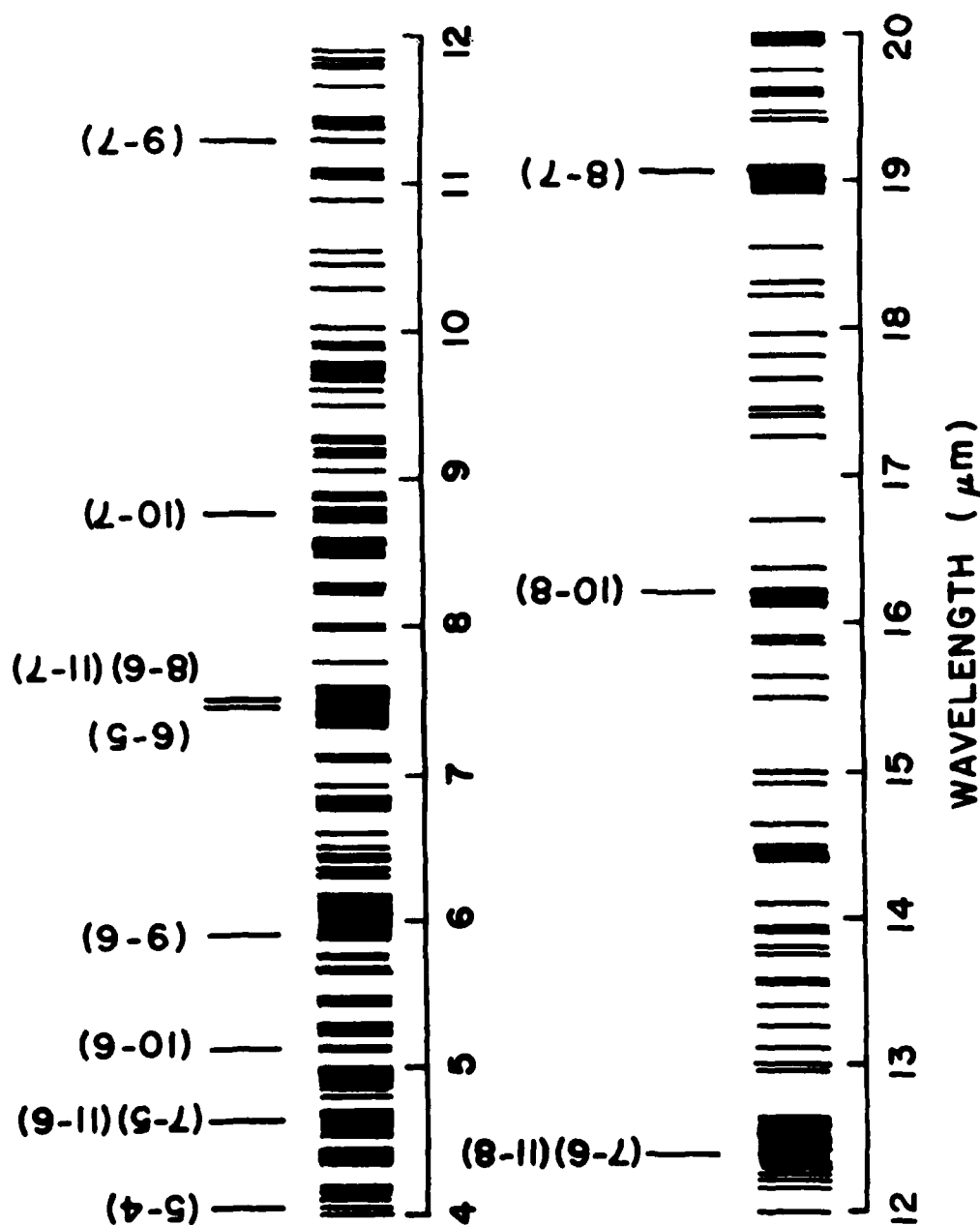


Figure 4. Possible infrared lines from transitions between singlet Rydberg states with $n < 11$. Numbers in parentheses indicate the hydrogenic lines of $n \rightarrow n'$ transition. (See text.)

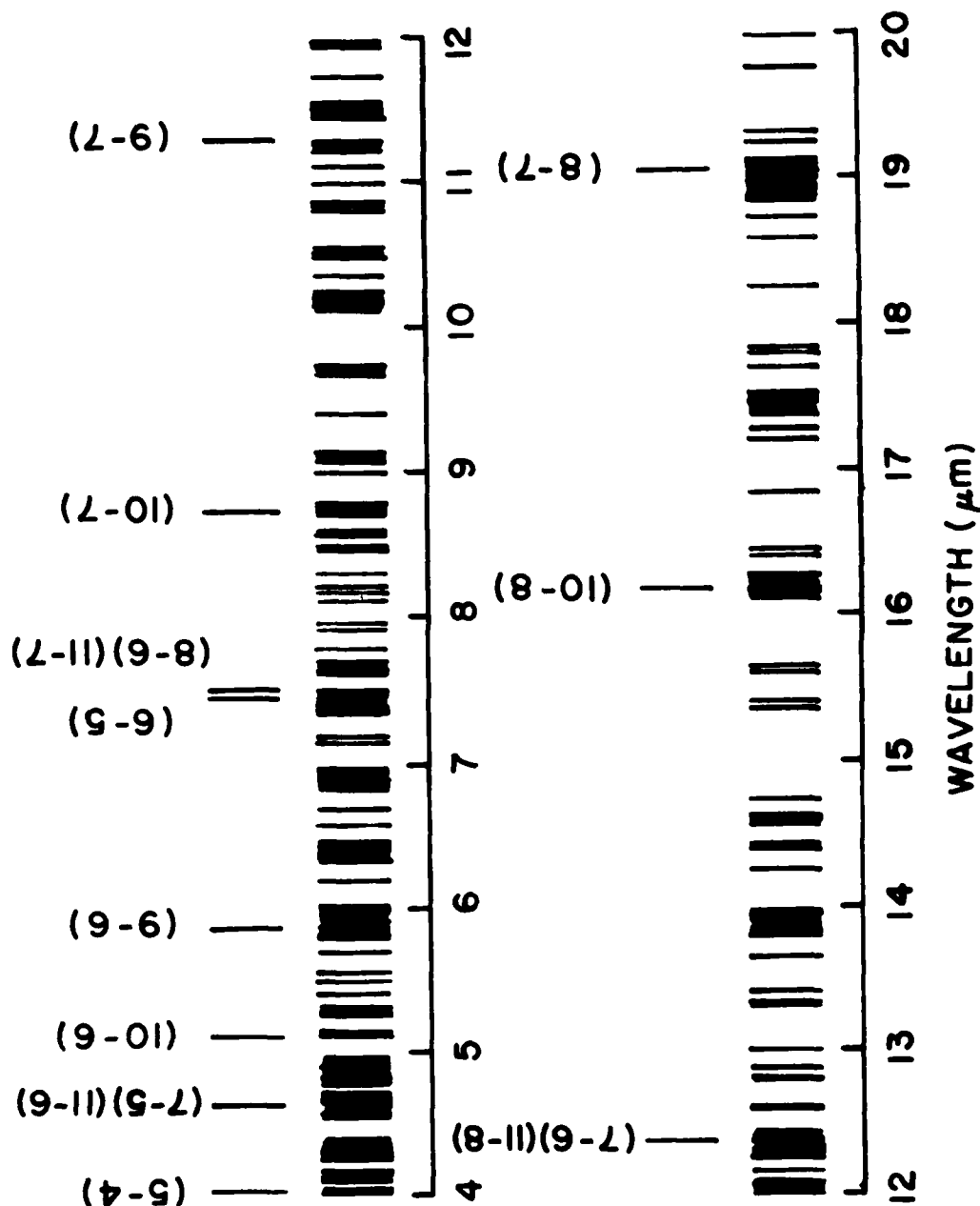


Figure 5. Possible infrared lines from transitions between triplet Rydberg states

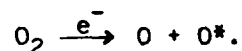
with $n \leq 11$. Numbers in parentheses indicate the hydrobenic lines of

$n \rightarrow n'$ transition. (See text.)

PART II

OPTICAL EXCITATION CROSS SECTION FOR EMISSION OF
LONG-WAVE INFRARED LINES OF ATOMIC OXYGEN PRODUCED
BY ELECTRON IMPACT ON OXYGEN MOLECULES

Long-wave infrared emission of atmospheric atoms, especially oxygen, is of great interest. One important mechanism for producing the "oxygen long-wave infrared emitters", i.e., highly excited oxygen atoms, is dissociation of O_2 by electron impact,



The ground state oxygen atom has an electron configuration $1s^2 2s^2 2p^4$. The excited states which lie below the first ionization limit are well described by the Russell-Saunders coupling. A configuration $2p^3 n\ell$ comprises a number of levels characterized by L, S, and J. In this work we are not concerned with the fine structure, thus we designate an excited level by n, ℓ , L, S.

An oxygen atom in a highly excited level, say $n=7$, may emit long-wave infrared radiation upon decaying to a level of slightly lower energy, say $n=6$. For example the $7f \ ^3F + 6d \ ^3D$ transition gives emission at 120,577 Å. However, measurement of the intensity of this emission is very difficult because the infrared detectors available for 120,000 Å wavelength have very low sensitivity compared to photomultipliers which operate in the wavelength range of about 2,000 - 12,000 Å.

Recently Schulman et al.¹ have performed experiments on production of excited oxygen atoms by electron impact on oxygen molecules with incident electron energy from threshold to 500 eV. They measured the intensity of radiation from the excited oxygen atoms in the wavelength range 3,690 - 11,300 Å corresponding to transitions from the highly excited states to the low excited states (3s and 3p). Absolute optical emission cross sections have been reported for transitions in the wavelength range 3,690 - 11,300 Å originating from some thirty spectroscopic terms. In this work we show that by combining the data of Schulman et al. with theoretical transition probabilities, it is possible to obtain optical cross sections for emission of atomic-oxygen lines in the long-wave infrared region (produced by electron impact on oxygen molecules) which are otherwise very difficult to measure directly.

The ratio of the optical emission cross sections for two transitions which originate from the same upper level is equal to the ratio of the corresponding transition probabilities A , i.e.,

$$Q(i \rightarrow j) = \frac{A(i \rightarrow j)}{A(i \rightarrow k)} Q(i \rightarrow k) . \quad (1)$$

Thus optical cross sections for the emission lines that share a common upper level with a transition reported in Ref. 1 can be determined by using the appropriate transition probabilities. Since direct measurement of emission intensity in the infrared, especially long-wave infrared, region is more difficult than in the visible and near ultraviolet region, Eq. (1) allows us to obtain optical cross sections for infrared lines from the theoretical transition probabilities.

In this section we consider only transitions between levels with the $2p^3(^4S)n\ell$ configuration. Since the O^+ core is in a 4S state, the total orbital angular momentum L of the oxygen atom is equal to ℓ . An excited level is then designated by $nLSJ$. The transition probability between two levels may be written as²

$$A(n'LSJ' \rightarrow nLSJ) = \mathcal{M}(M)\mathcal{M}(L)a(n'L'S \rightarrow nLS)/(2J'+1), \quad (2)$$

$$a(n'L'S \rightarrow nLS) = 64\pi^4 \nu^3 \sigma^2 / 3hc^3, \quad (3)$$

$$\sigma^2 = e^2 \left| \int R_{n\ell}(r) r R_{n'\ell'}(r) r^2 dr \right|^2 / (4\ell_{>}^2 - 1), \quad (4)$$

where $\mathcal{M}(M)$ is the multiplet strength, $\mathcal{M}(L)$ the line strength, $R_{n\ell}$ the radial wave function, and $\ell_{>}$ is the greater of ℓ and ℓ' . Formulas for $\mathcal{M}(M)$ and $\mathcal{M}(L)$ are given in Ref. 3. For transitions between states of the type $2p^3(^4S)n\ell$, the values of $\mathcal{M}(M)$ are 15 for $^5S-^5P$, 150 for $^5P-^5D$, 525 for $^5D-^5F$, 9 for $^3S-^3P$, 90 for $^3P-^3D$, and 315 for $^3D-^3F$. The line strengths are shown in Table I.

The radial wave functions $R_{nl}(r)$ in Eq. (4) are calculated by the Hartree-Fock self-consistent-field (SCF) procedure. To simplify the calculation, the 1s and 2s orbitals of the excited oxygen atom are taken from the SCF solution of the $O^+[2p^3(^4S)]$ ion, and are not varied in the iteration cycles. In Table II we list the values of $a(n'L'S \rightarrow nLS)$ calculated from these Hartree-Fock wave functions for the transitions which are used to obtain the long-wave infrared emission cross sections according to Eq.(1). For a given configuration $2p^3(^4S)nl$, the radial wave functions for the triplet states are different from those for the quintet states because of the different exchange terms in the Fock equations. This is particularly true for the np series on account of the strong exchange interaction between the 2p and np orbitals. We see in Table II that this difference in radial functions between the triplet and quintet series is reflected in the transition probabilities.

To get an indication of the accuracy of the Hartree-Fock calculation, we have computed the transition probabilities using a different method, i.e., the self-interaction-corrected form of the local-spin-density (LSD) approximation. This method has been discussed extensively in the literature,⁴⁻⁷ thus only a brief description is presented here. In the conventional LSD or the Hartree-Fock-Slater method, the exchange potential in the Fock equations for the one-electron orbitals is approximated by a local potential proportional to the cubic root of the electron density (or spin density for spin-polarized cases), $\rho^{1/3}$. This local exchange approximation greatly simplifies the computational work, but has a serious drawback related to the self-interaction in the following way. The effective potential of an electron in the Hartree-Fock theory consists of the electron-nucleus attraction, electron-electron Coulomb repulsion, and the exchange potential. The electron-

electron Coulomb repulsion includes a term corresponding to the interaction of the electron with itself. This unphysical self-interaction is cancelled by an identical term in the exchange potential so that its presence has no effect. However, when the exchange potential is approximated by the local $\rho^{1/3}$ form, the cancellation of the self-interaction energy is not complete. One troublesome consequence of this incomplete cancellation is that for a neutral atom the electron potential at a large distance r from the nucleus approaches zero much faster than the correct $-1/r$ dependence, resulting in an underestimation of the net attraction, hence the ionization energy. This difficulty is partly resolved by a cutoff procedure, adopted in the Herman-Skillman formulation⁸ of the Hartree-Fock-Slater method, in which the local exchange approximation is used only in the region of r between zero and a cut-off value r_0 , and for $r > r_0$ the electron potential is simply set to $-1/r$. Nevertheless this cutoff procedure does not completely remove the spurious self-interaction, although it gives the correct asymptotic potential energy.

A more fundamental way of addressing the problem of self-interaction is to remove the self-interaction terms from the total energy in the outset. This approach has recently met with great success in calculations of electronic structure of atoms,⁴⁻⁶ and is often referred to as the self-interaction correction (SIC). Of special interest to us is the paper of Harrison *et al.*,⁷ which demonstrates the success of the SIC-LSD approximation for calculating energies of excited states of atoms. The SIC-LSD approximation retains the computational simplicity of the Hartree-Fock-Slater approach, but provides a significant improvement over the conventional LSD approximation.

We have applied the SIC-LSD method (spin-polarized) to calculate $a(n'L'S + nLS)$ for the quintet states,⁹ and the results agree well ($\sim 10\%$)

with the values obtained by the Hartree-Fock wave functions (Table II).

The agreement between the two sets of results supports the accuracy of our calculation within the Hartree-Fock framework.

Earlier works on the transition probabilities of the oxygen atom include the calculation using wave functions determined by the Hartree-Fock-Slater method (without the SIC).¹⁰ The formulation of the Hartree-Fock-Slater method as given in Ref. 8 uses the total electron density (rather than the spin density) in the $\rho^{1/3}$ -exchange term; therefore it gives the same $R_{nl}(r)$ for the quintet and triplet states of the $2p^3(4S)nl$ configurations. Nevertheless, compared with our values of σ [Eq. (4)] of the quintet series, those of Ref. 10 are generally within a 25% range when σ is greater than 1.0. For smaller values of σ the discrepancy is much larger. As pointed out in Ref. 10, the integral of Eq. (4) is very sensitive to the wave functions, particularly when severe cancellation occurs between the positive and negative contributions. Thus it is not surprising to find a much larger discrepancy between the Hartree-Fock and Hartree-Fock-Slater results for the cases where σ is small.

Biemont and Grevesse¹¹ calculated oscillator strengths for a large number of infrared lines of atomic oxygen using the Coulomb approximation.^{12,13} The Coulomb approximation takes advantage of the fact that, in the usual length formula, nearly all the contribution to the dipole matrix element comes from the outer lobes of the two wave functions involved. This asymptotic part of the wave function may be computed simply with the knowledge of the Coulombic potential and the ionization energy, since the short-range potentials such as electron-exchange potential become negligible for large r . Therefore, this method is suitable for computing the dipole matrix elements between a pair of highly excited states. It follows, on the other hand, that the validity of this method may be questioned for low-lying

states, and this point is discussed in Ref. 12.

The majority of the infrared lines of Ref. 11 involve highly excited states. Comparison is made of σ^2 in Eq. (4) between the present work and Ref. 11 for some 140 transitions (ns, np, nd, and nf, with n up to 10). In most cases the agreement is within 25%. About ten cases, in which discrepancy is greater than 25%, occur mostly in $^3S - ^3P$ and $^3P - ^3D$ series.

In computing dipole matrix elements, the relative "phase" of the pair of wave functions is an important factor. The position of the outer peak of a wave function is dictated by the details of the potential in the interior region. In our Hartree-Fock calculation the triplet and quintet functions of the same nl are shifted relative to each other because of the difference in exchange-coupling coefficients. When the Coulomb approximation is used, such effect is taken into consideration to some extent through the effective quantum number n^* , but falls short of the rigorous treatment with the result that the wave function may be shifted by an improper amount from the hydrogenic counterpart. Although the inaccuracy in the phase shift may be small in each of the wave functions, it could lead to much greater error in the dipole matrix elements where the relative phase shift of the two functions is an important factor. The discrepancy in the $^3S - ^3P$ and $^3P - ^3D$ series referred to in the preceding paragraph may be attributed to the inaccuracy in the phase shift in the Coulomb-approximation wave functions.

The values of $a(n'L'S \rightarrow nLS)$ in Table II are combined with the measured optical emission cross sections of Ref. 1 in accordance with Eq. (1) to yield optical cross sections for a number of infrared lines. Since the individual $J' \rightarrow J$ components of an $n'L'S \rightarrow nLS$ transition are not resolved in the measured emission, we assume that the population of the J-levels (due to electron impact) within an (nLS) term is proportional to the statistical

weight, $2J+1$. The optical cross sections for fifteen $n'L'S \rightarrow nLS$ transitions in the 40,000-140,000 Å range obtained in this way are summarized in Table III.

REFERENCES

1. M. Bruce Schulman, Francis A. Sharpton, Sunggi Chung, Chun C. Lin, and L. W. Anderson, Phys. Rev. A 32, 2100 (1985).
2. E. U. Condon and G. H. Shortley, The Theory of Atomic Spectra, (Cambridge University Press, 1963).
3. R. Rohrllich, Astrophys. J. 129, 441 (1959).
4. I. Lindgren, Int. J. Quantum Chem. Symp. 5, 411 (1971).
5. J. P. Perdew, Chem. Phys. Lett. 64, 127 (1979).
6. J. P. Perdew and A. Zunger, Phys. Rev. B 23, 5048 (1981).
7. J. G. Harrison, R. A. Heaton, and C. C. Lin, J. Phys. B 16, 2079 (1983).
8. F. Herman and S. Skillman, Atomic Structure Calculations (Prentice-Hall, Englewood Cliffs, N. J., 1963).
9. Application of the SIC-LSD approximation to calculate the SCF orbitals is much more difficult for the triplet states of the $2p^3(^4S)n\ell$ configurations since these states, unlike the quintet states, cannot be represented by a single-determinant wave function.
10. P. S. Kelly, J. Quant. Spectros. Radiat. Transfer 4, 117 (1964).
11. E. Biemont and N. Grevesse, At. Data Nucl. Data Tables 12, 217 (1973).
12. D. R. Bates and A. Damgaard, Philos. Trans. R. Soc. London 242, 101 (1949).
13. H. Friedrich, K. Katterbach, and E. Trefftz, J. Quant. Spectrosc. Radiat. Transfer 10, 11 (1970).

Table 1. Line Strength $f(L)$

54

Quintets (S=2)				Triplets (S=1)			
	J'	J	$f(L)$		J'	J	$f(L)$
S-P	2	3	7/15		1	2	5/9
	2	2	1/3		1	1	1/3
	2	1	1/5		1	0	1/9
P-D	3	4	9/25		2	3	7/15
	3	3	7/75		2	2	1/12
	3	2	1/75		2	1	1/180
	2	3	14/75		1	2	1/4
	2	2	7/60		1	1	1/12
	2	1	3/100		0	1	1/9
	1	2	7/100				
	1	1	9/100				
	1	0	1/25				
D-F	4	5	11/35		3	4	3/7
	4	4	3/70		3	3	1/27
	4	3	1/350		3	2	1/945
	3	4	3/14		2	3	8/27
	3	3	3/50		2	2	1/27
	3	2	1/175		1	2	1/5
	2	3	24/175				
	2	2	2/35				
	2	1	1/175				
	1	2	2/25				
	1	1	1/25				
	0	1	1/25				

Table II. $a(n'L'S \rightarrow nLS)$ as defined in Eq. (3).

O Multiplet	$\lambda(\text{\AA})$	$a \text{ (sec}^{-1}\text{)}$
$6s \ ^5S \rightarrow 3p \ ^5P$	5437.45	1.28824 (6)^a
$6s \ ^3S \rightarrow 3p \ ^3P$	6048.06	1.05174 (6)
$6s \ ^5S \rightarrow 5p \ ^5P$	71779.87	5.44747 (5)
$6s \ ^3S \rightarrow 5p \ ^3P$	77211.17	4.49093 (5)
$7s \ ^5S \rightarrow 3p \ ^5P$	5020.83	7.12077 (5)
$7s \ ^5S \rightarrow 6p \ ^5P$	132148.12	2.09108 (5)
$4p \ ^5P \rightarrow 3s \ ^5S$	3948.57	3.50477 (5)
$4p \ ^5P \rightarrow 3d \ ^5D$	59773.34	4.93382 (4)
$5d \ ^5D \rightarrow 3p \ ^5P$	5331.32	4.54278 (5)
$5d \ ^5D \rightarrow 4f \ ^5F$	41371.10	2.85093 (3)
$5d \ ^5D \rightarrow 5p \ ^5P$	56842.49	2.76437 (5)
$7d \ ^5D \rightarrow 3p \ ^5P$	4774.37	1.17938 (5)
$7d \ ^5D \rightarrow 5f \ ^5F$	46907.72	1.09355 (3)
$7d \ ^5D \rightarrow 6p \ ^5P$	56026.60	4.03733 (4)
$7d \ ^5D \rightarrow 6f \ ^5F$	126850.42	1.39241 (3)
$6f \ ^5F \rightarrow 3d \ ^5D$	10678.77	1.57035 (5)
$6f \ ^3F \rightarrow 3d \ ^3D$	10756.48	1.50984 (5)
$6f \ ^5F \rightarrow 5d \ ^5D$	71440.57	5.01200 (4)
$6f \ ^3F \rightarrow 5d \ ^3D$	72664.23	5.12763 (4)
$7f \ ^5F \rightarrow 3d \ ^5D$	9828.63	8.86534 (4)
$7f \ ^3F \rightarrow 3d \ ^3D$	9894.46	8.47534 (4)
$7f \ ^5F \rightarrow 5d \ ^5D$	45254.09	3.01991 (4)
$7f \ ^3F \rightarrow 5d \ ^3D$	45742.75	3.01714 (4)
$7f \ ^5F \rightarrow 6d \ ^5D$	118529.35	1.76778 (4)
$7f \ ^3F \rightarrow 6d \ ^3D$	120577.23	1.83095 (4)

^a Numbers in the parentheses denote the power of 10.

Table III. Excitation cross sections for long-wave infrared emission
of O produced by dissociative electron-impact excitation of O₂ at 100 eV.

O Multiplet	$\lambda(\text{\AA})$	$\Sigma_{J', J''_{\text{opt}}(J' \rightarrow J)}$ (10 ⁻²⁰ cm ²)
5d ⁵ D ^o → 4f ⁵ F	41371	0.075
7f ⁵ F → 5d ⁵ D ^o	45254	0.82
7f ³ F → 5d ³ D ^o	45743	0.53
7d ⁵ D ^o → 5f ⁵ F	46908	0.019
7d ⁵ D ^o → 6p ⁵ P	56027	0.20
5d ⁵ D ^o → 5p ⁵ P	56842	2.1
4p ⁵ P → 3d ⁵ D ^o	59773	2.9
6f ⁵ F → 5d ⁵ D ^o	71441	1.4
6s ⁵ S ^o → 5p ⁵ P	71780	0.33
6f ³ F → 5d ³ D ^o	72664	1.3
6s ³ S ^o → 5p ³ P	77211	0.13
7f ⁵ F → 6d ⁵ D ^o	118529	0.48
7f ³ F → 6d ³ D ^o	120577	0.32
7d ⁵ D ^o → 6f ⁵ F	126850	0.024
⁵ S ^o → 6p ⁵ P	132148	0.085

PUBLICATIONS

The following paper has been published under the sponsorship of this contract

1. Sunggi Chung, Chun C. Lin, and Edward T.P. Lee, J. Chem. Phys. 82, 342 (1985).
2. M. Bruce Schulman, Francis A. Sharpton, Sunggi Chung, Chun C. Lin, L. W. Anderson, Phys. Rev. A 32, 2100 (1985).
3. Sunggi Chung, Chun C. Lin, and Edward T. P. Lee, J. Quan. Spectrosc. Radiat. Transfer, in press.

END
FILMED

5-86

DTIC